Accurate Determination of the Structure of Cyclooctatetraene by Femtosecond Rotational Coherence Spectroscopy and ab Initio Calculations

Dominique S. Kummli, Simon Lobsiger, Hans-Martin Frey, and Samuel Leutwyler*

Departement für Chemie and Biochemie, Universität Bern, Freiestrasse 3, CH-3000 Bern 9, Switzerland

John F. Stanton

Department of Chemistry and Biochemistry, University of Texas at Austin, Austin, Texas 78712

Received: April 23, 2008; Revised Manuscript Received: July 8, 2008

We combine femtosecond time-resolved rotational coherence spectroscopy with high-level ab initio theory to obtain accurate structural information for the nonpolar antiaromatic molecule 1,3,5,7-cyclooctatetraene (C_8H_8, COT) and its perdeuterated isotopomer COT-d_8 (C_8D_8). We measure the rotational B_0 and centrifugal distortion constants D_J, D_{JK} of the $v = 0$ states of COT and COT-d_8 to high accuracy, e.g. B_0 (COT) = 2710.329(56) MHz, as well as B_v for the $v = 1$ states ν_6, ν_{11}, ν_{17}, ν_{22}, and ν_{41}/ν_{42} of COT. The experimental rotational constants are compared to those obtained from calculations at the coupled-cluster with single, double, and perturbative triples [CCSD(T)] level. The latter also take into account vibrational averaging effects of the ground and vibrationally excited states. Combining the experimental and calculated rotational constants with the calculated equilibrium bond lengths and angles allows us to determine accurate equilibrium structure parameters, e.g., r_e (C−C) = 147.0 ± 0.05 pm, r_e (C═C) = 133.7 ± 0.1 pm, and r_e (C−H) = 107.9 ± 0.1 pm. The equilibrium C−C and C═C bond lengths of COT are compared to those of 1,3-butadiene. The expected effect of decreased π-electron delocalization due to the twisting of adjacent C═C double bonds in COT relative to butadiene is observed for the C−C bonds but not for the C═C bonds.

I. Introduction

The determination of accurate molecular structures has been one of the central endeavors of chemistry for many decades.[1−3] In the gas phase, different high-resolution spectroscopic methods have been applied to measure molecular structures via the determination of the rotational constants.[2,3]

Cyclooctatetraene (COT) is a prototype antiaromatic system.[4−15] Accordingly, distribution of the eight π electrons in the molecule orbitals derived from a D_{8h} (regular octagonal) structure does not lead to a closed-shell determinant. Accordingly, vibronic effects act to lower the energy when the geometry is distorted from this high symmetry, and a lower symmetry equilibrium geometry results. This is similar to the case of the simpler 4*n* antiaromatic cyclobutadiene, but COT is somewhat less well understood. While negative ion photoelectron spectroscopy in particular[16] has revealed a great deal of information about the electronic structure of COT, less is known about its structure apart from the point group symmetry, which has been established to be a D_{2d}-symmetric tub-shaped equilibrium structure in which two pairs of carbon atoms are bent downward and two pairs upward from a structure with D_{4h} symmetry.[10,11] The barrier between the two forms differing in the identity of the "up" and "down" carbons is substantial. A calculation at the MP2/6-31G(d,p) level predicts an inversion barrier of 17.1 kcal/mol (5980 cm^{-1}).[11] For a unique structure determination, six internal coordinates have to be known, i.e., the C−C, C═C, and C−H bond lengths together with the C−C═C, C═C−H, and C−C−H angles, denoted α, β, and γ, see Figure 1.

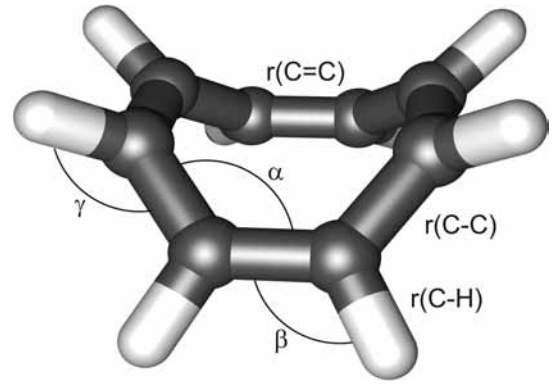

Figure 1. Schematic D_{2d} equilibrium structure of cyclooctatetraene.

Because COT lacks a permanent dipole moment, it is not possible to employ microwave spectroscopy - the most precise gas-phase structural method - for the determination of its rotational constants. Structural information on cyclooctatetraene has been obtained from electron diffraction (ED) measurements.[17−22] The earliest geometry determination by ED was based on a D_{4d} symmetric structural model with equivalent C−C bond lengths and a C−C−C angle of 120°.[17] Kaufman et al. measured the X-ray structure of solid COT and for the first time reported the correct D_{2d}-symmetric tub form with alternating C−C and C═C bonds.[23] The X-ray structure was later refined at 129 K by Claus and Krüger to values of 147.0(2) and 133.3(2) pm for the C−C and C═C bond lengths; the C−C═C angle was determined to 126.6(1)°.[24]

A number of Raman[5−8,18,25,26] and infrared (IR)[6−8,17,25,26] spectroscopic studies on COT addressed the determination of its point-group symmetry. Most of these early analyses led to

* To whom correspondence should be addressed. E-mail: leutwyler@iac.unibe.ch.

10.1021/jp803523y CCC: $40.75
Published on Web 08/28/2008

D_4 or D_{4d} symmetry. Perec provided a normal-mode calculation and reanalysis of the IR spectrum of COT and COT-d_8 based on D_{2d} symmetry and revised assignments of the fundamental modes for both compounds.[27] Rotationally resolved infrared spectroscopy can give very accurate rotational constants for small molecules. However, COT is sufficiently large such that the corresponding rotational levels are so tightly spaced as to thus far have prevented structural analysis by these means. Thomas and Weber have recorded the rotationally resolved Raman spectrum of C_8H_8 and determined the B_0 rotational and D_J centrifugal distortion constants.[28] They calculated the moment of inertia based on the structural parameters of Haugen and Traetteberg[22] and compared the value with their Raman B_0 constant.

Several ab initio studies of the ground-state structure, the ring-puckering intrinsic reaction coordinate, and barrier height have been performed.[10,11,15,29−33] Andres et al. optimized the structure at the CASSCF/6-31G* level and studied six energetically low-lying conformers and/or transition structures.[11] In a study of the electronic excitations of COT, Merchan et al. reoptimized the CASSCF ground-state equilibrium structure with a larger ANO basis set.[32] Petryk et al. optimized the equilibrium D_{2d} geometry with density functional theory and the Dunning cc-pVXZ ($X = 2, 3, 4$) basis sets.[33] Later computational work addressed aspects of the ring-puckering deformation induced by vibronic (pseudo Jahn−Teller) couplings.[15,31]

Time-resolved femtosecond degenerate four-wave mixing (fs-DFWM) can be used as a Raman scattering type of rotational coherence spectroscopy (RCS).[34−38] It is a background-free Raman rotational technique that permits the highly accurate determination of rotational and centrifugal distortion constants of molecular ground states[37−51] and of thermally populated low-lying vibrational states.[52,53] Following our studies on nonpolar cycloalkanes,[50,51,53] we here investigate the nonpolar cycloalkene COT and COT-d_8 (C_8D_8). We report accurate rotational and centrifugal distortion constants of the ground, the five vibrationally excited states ν_6, ν_{11}, ν_{17}, and ν_{22} and the degenerate ν_{41}/ν_{42} pair of COT and the rotational and centrifugal distortion constant of the ground-state of COT-d_8.

In parallel, we employ ab initio theory at the CCSD(T) (coupled-cluster including singles, doubles, and iterative triples) level to calculate the optimized ground-state equilibrium structure of COT as well as its vibrationally averaged structure and rotational constants for the ground ($v = 0$) and vibrationally excited ($v = 1$) states. Combining the experimental results with a basis-set extrapolation technique[50,52,53] allows us to obtain the equilibrium structure of cyclooctatetraene to high accuracy.

II. Methods

A. Experimental. The experimental setup employed for recording fs-DFWM transients has been described earlier.[43,50,52] Briefly, the 800 nm output of a Ti:sapphire oscillator is amplified with a Quantronix femtosecond chirped-pulse amplifier at 1000 Hz repetition rate. The temporal and bandwidth properties of the fs pulses were characterized as 75 fs fwhm, 0.45 time bandwidth product, 12.63 nm bandwidth using a single-shot second-harmonic-generation frequency-resolved Grenouille optical gating device. The probe beam runs over a 1 in. diameter retroreflector mounted on a computer-controlled 600 mm long delay stage. Displacements are measured with a 600 mm glass ruler (Sony BL55-NEA) with a resolution of 100 nm. The optical delay line is enclosed in a vacuum-tight container and evacuated to $\leq 5 \times 10^{-2}$ mbar using a scroll pump (Varian Triscroll 300).[50] The two pump and the probe beams are focused by a 1000 mm lens in a forward box configuration into a stainless-steel cell containing the gaseous sample.

Cyclooctatetraene (Fluka, 97% purity) was used without further purification. Cyclooctatetraene-d_8 (Cambridge Isotope Laboratories Inc., 97−98% isotopic purity and 89.5% chemical purity) was purified from benzene-d_6 by a 5-fold destillation. The remaining ~1% impurity of benzene-d_6 could not be removed any further. Measurements were performed at 3−5 mbar. The pressure was measured with an MKS Baratron capacitance gauge accurate to ±0.1 mbar.

The generated four-wave mixing signal is detected with a thermoelectrically cooled Hamamatsu 7422−50 photomultiplier. The signals were digitized with a LeCroy Wave Runner LT372 transient digitizer, scaled, combined and stored in a PC. For the transients of COT and COT-d_8, the time delay was scanned in overlapping regions covering 4 recurrences at a time in steps of 20.0 fs. The laser pulse energy was set to 5−20 μJ per beam for the COT measurements and to 15−40 μJ for COT-d_8. We were able to record 35 COT and 20 COT-d_8 recurrences over a total scan length of 3260 and 1340 ps, respectively. For COT, the DFWM signal is limited by the overall signal decay due to collisional dephasing (see below). The usable transient of COT-d_8 was limited to 1340 ps by the interferences of the recurrences from the remaining ~1% impurity of benzene-d_6 with the COT-d_8 recurrences.

B. Calculations. Ab initio calculations were carried out using the coupled-cluster singles and doubles method[54] with perturbative treatment of triple excitations, CCSD(T).[55] The geometry of COT was optimized at this level of theory using analytic gradient methods[56] with Dunning's cc-pVDZ and cc-pVTZ basis sets and the ANO0 basis set, which has precisely the same number and types of contracted functions as cc-pVDZ.[57] Experience has shown that the ANO basis sets do an excellent job of treating molecular force fields, with performance that is usually superior to the comparable contraction size in the cc-pVXZ hierarchy, especially with the smallest members.[58] The harmonic and cubic force fields of COT were computed at the CCSD(T) level with the ANO0 basis using analytic second derivative techniques.[59] These calculations were carried out with the Mainz-Austin-Budapest version of the ACES II program package.[60] Core electrons were omitted from the correlation treatment in all calculations.

III. DFWM Theory and Data Analysis

A. Vibrational and Rotational States and Level Populations. Simulations of fs-DFWM transients[50,52] as well as the underlying theory[61−64] are well established and only briefly reviewed here. Three polarized laser beams of equal intensity are focused in a forward box configuration into a Raman-active medium. Two pump pulses (E_1, E_2) induce an anisotropy by rotational Raman transitions in the medium. This anisotropy is probed via a third order optical process. The probe beam (E_3) generates a four-wave mixing signal at times when the molecules are aligned. The time-dependent third order polarization is given by

$$P^{(3)}(t) = E_3(t)\int_{-\infty}^{\infty} E_1(t)E_2(t)\sum^{N} p_v\, p_{J,K} g_J g_{v,K,NS} b_{J'K'JK} e^{-k_{J,K}t} e^{i\Delta\omega_{J,K}t}\, dt \quad (1)$$

involving a sum over the N populated levels. The squared norm of the third order polarization, $|P^{(3)}(t)|^2$ together with eq 1 in combination with the level dependent transition probabilities leads to the transient recorded.

TABLE 1: Cyclooctatetraene and Cyclooctatetraene d_8 Vibrations, Their Irreducible Representations, Anharmonic Frequencies (cm^{-1}), and Vibrational Populations (in %)

		COT		COT-d_8	
mode	irrep	frequency[a]	population[b]	frequency[a]	population[b]
$\upsilon = 0$	a_1		20.0		14.6
ν_6	a_1	182.5	8.2	157.2	6.8
ν_{11}	a_2	233.7	6.4	211.4	5.2
ν_{17}	b_1	258.3	5.7	244.7	4.4
ν_{22}	b_2	289.2	4.9	262.0	4.1
$\nu_{41/42}$	e	363.4	6.8	304.9	6.6
$2\nu_6$	a_1			313.7	3.2

[a] Anharmonic B3LYP/cc-pVTZ frequencies. [b] Percent of the total population.

TABLE 2: Statistical Weights $g_{K,NS}$ of Cyclooctatetraene (C_8H_8) for the a_1, a_2, b_1, b_2, and e Vibrational States

	vibrational level				
rotational state	a_1 ($\upsilon = 0$, ν_6=1)	a_2 ($\nu_{11} = 1$)	b_1 ($\nu_{17} = 1$)	b_2 ($\nu_{22} = 1$)	e ($\nu_{41,42} = 1$)
$K = 0$, J even	76	60	76	60	120
$K = 0$, J odd	60	76	60	76	120
$K = 4p$	136	136	136	136	240
$K = 4p \pm 1$	120	120	120	120	272
$K = 4p \pm 2$	136	136	136	136	240
$K = 4p \pm 3$	120	120	120	120	272

Vibrational Population p_υ. At the experimental temperature $T = 295$ K only 20% of all molecules are in the vibrational ground state. Table 1 shows the B3LYP/cc-pVTZ calculated anharmonic frequencies, irreducible representations and population factors of the vibrations that are relevant for the analysis of the transients of COT and COT-d_8. The degeneracy of the $\nu_{41/42}$ vibration mode is contained in the factor $g_{\upsilon,K,NS}$, see below. Because the DFWM signal is proportional to the square modulus of $P^{(3)}(t)$, the contributions of the vibrationally excited states to the transient are not simply added to the dominant $\upsilon = 0$ signal. Mutual interference terms arise between all these terms according to eq 1, as shown below.

Rotational Population $p_{J,K}$. The $t = 0$ initial rotational populations $p_{J,K}$ in eq 1 are determined via the Boltzmann distribution by the rotational term values $E_{J,K}$ (see eq 2) and the sample temperature T. We fitted the $E_{J,K}$ according to the standard oblate symmetric top formula including quartic centrifugal distortion terms (note the υ-dependence of the rotational constants)

$$E_{J,K} = B_\upsilon J(J+1) + (B_\upsilon - C_\upsilon)K^2 - D_{J,\upsilon} J^2(J+1)^2 - D_{JK,\upsilon} J(J+1)K^2 - D_{K,\upsilon}K^4 \quad (2)$$

For symmetric rotors, the M_J spatial degeneracy is $g_J = 2J + 1$ (see eq 1). Due to the high inversion barrier, the interconversion tunneling between the two degenerate ground-state structures is much slower than the molecular rotation, therefore the nuclear spin states of COT and COT-d_8 are treated in the rigid-molecule point group D_{2d}. The statistical weights due to the vibrational degeneracy, the rotational K-degeneracy and the nuclear spin weights, $g_{\upsilon,K,NS}$ in eq 1, were evaluated using the software package for group theory (GAP)[65,66] and the irreducible representations Γ_{rve} given by Weber.[67] For convenience, the $g_{\upsilon,K,NS}$ statistical weights are given for for COT in Table 2 and for COT-d_8 in Table 3, for the different K rotational states and all irreducible representations of the D_{2d} group. Note that $g_{\upsilon,K,NS}$ includes the degeneracy factor for the e vibrations and the K degeneracy of 2 for the $K \neq 0$ states (which is not clearly indicated in ref. 61). Since the C_υ and $D_{K,\upsilon}$ constants are experimentally not accessible (they cancel when calculating Raman transition frequencies), values of a B3LYP/cc-pVTZ calculation were used to calculate the rotational populations. The rotational Raman intensities for anisotropic Raman scattering, $b_{J'K'JK}$ in eq 1, are described with the Clebsch-Gordan formalism[68] and are included according to Weber[69] for the O, P, R, and S transitions.

TABLE 3: Statistical Weights $g_{K,NS}$ for Cyclooctatetraene-d_8 (C_8D_8) for a_1, a_2, b_1, b_2, and e Vibrational States

	vibrational level				
rotational state	a_1 ($\upsilon = 0$, $\nu_6 = 1$)	a_2 ($\nu_{11} = 1$)	b_1 ($\nu_{17} = 1$)	b_2 ($\nu_{22} = 1$)	e ($\nu_{41,42} = 1$)
$K = 0$, J even	1701	1620	1701	1620	3240
$K = 0$, J odd	1620	1701	1620	1701	3240
$K = 4p$	3321	3321	3321	3321	6480
$K = 4p \pm 1$	3240	3240	3240	3240	6642
$K = 4p \pm 2$	3321	3321	3321	3321	6480
$K = 4p \pm 3$	3240	3240	3240	3240	6642

The finite temporal and spectral bandwidth of the fs laser has two distinct effects on the transient: (i) The transient has to be convoluted with the three fs laser pulse widths. The experimentally measured zero-time Kerr-peak of Ar gas directly yields this self-convolution of the three pulses. The corresponding apparatus function is very closely represented by a Gaussian with 155 fs fwhm (full width at half-maximum). (ii) The Raman processes are limited to transitions within the spectral bandwidth of the laser, which is measured to be 160 cm^{-1}, see section II.

B. Rotational Energy Transfer. As discussed above, the initial rotational state distribution at $t = 0$ is given by the Boltzmann distribution at the sample temperature $T = 295$ K. Following the pump/dump pulses at $t = 0$, the rotational coherence of the sample is destroyed due to R $\leftrightarrow$ R and R $\leftrightarrow$ T collisions that change the rotational state and/or phase. In eq 1 this dephasing is accounted for by the exponential term $e^{-k_{J,K}t}$ where $k_{J,K}$ is the dephasing rate of a given J,K rotational state and is modeled according to the energy gap law model for collisional rotational energy transfer (RET), $k_{J,K} = ae^{-c\Delta E_J}$. In the RET model, a and c are coefficients to be fitted, $\Delta E_{J,\upsilon} = |E_{J\pm1,\upsilon} - E_{J,\upsilon}| = 2B_\upsilon J$ is the rotational level spacing and B_υ is the rotational constant.[70,71] In fs-DFWM work on cyclopropane and cyclobutane we considered only $\Delta J = \pm 1$ processes, since this accounted for the observed RCS transient in a satisfactory way.[52,53] For COT and COT-d_8, this rotational dephasing model is only able to reproduce the observed transient up to $t \leq 1500$ ps. Employing exclusively K-changing transitions did not improve the situation. An extended model which focuses on J-changing transitions with the inclusion of the two closest lying K-changing transitions shows improved behavior, i.e., when fitting the temperature, it remains close to 300 K for delay times up to $t = 3300$ ps.

IV. Results

A. DFWM Measurements, Fitting and Rotational Constants of C_8H_8. Figures 2 and 3 show the Raman RCS transient of C_8H_8 over the time ranges $t = 80-1880$ and 1930−3260 ps, respectively. The large Kerr-effect signal at time zero is off the scale of Figure 2 and is not shown. The rotational Raman contribution to the signal near time zero also provides information on the rotational constants,[38] but the information is much less accurate than that obtained from the later transients. In the integer recurrences (Figures 2 and 3), interference occurs

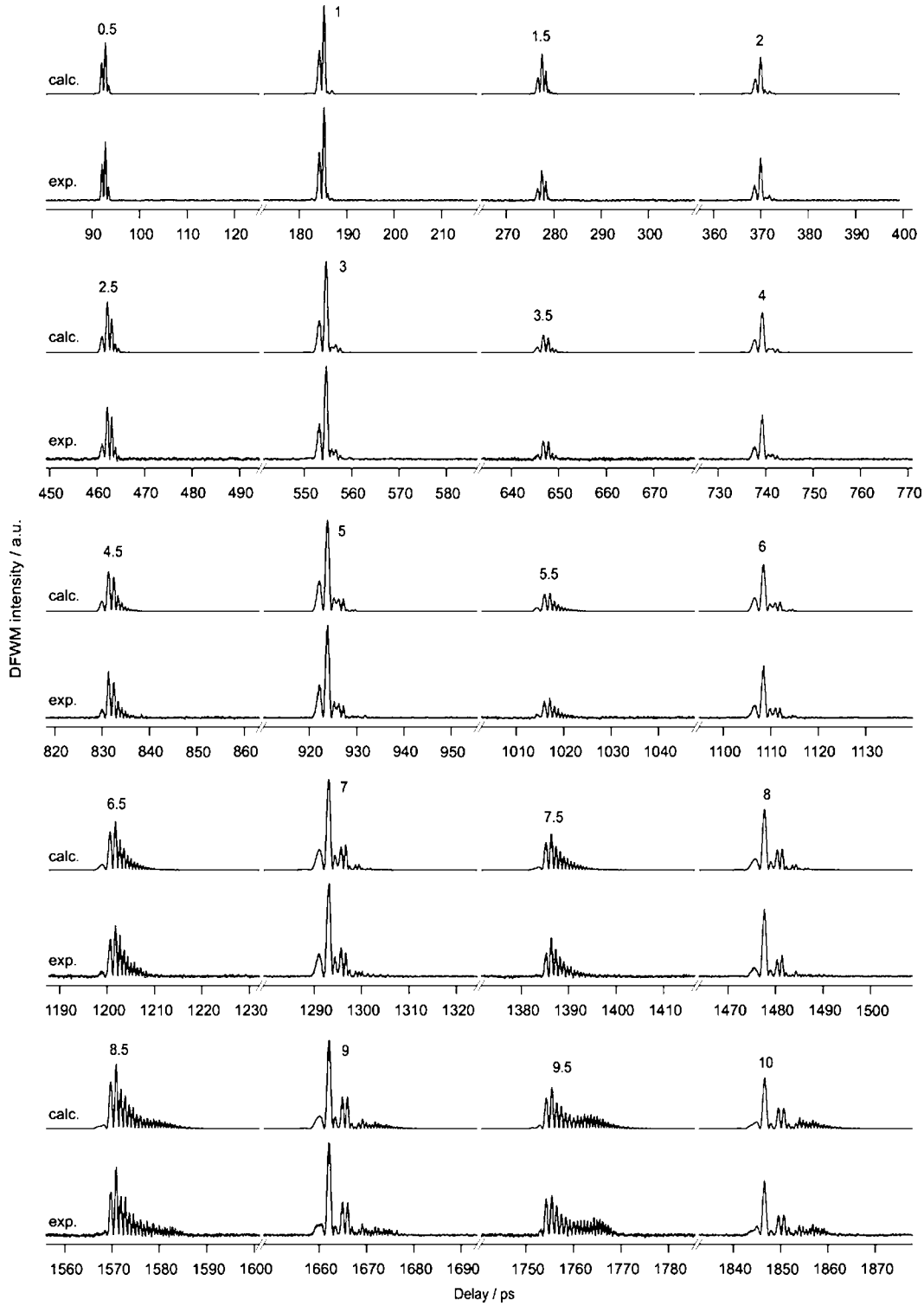

Figure 2. fs-DFWM rotational coherence transient of COT in a gas cell (295 K, $p = 3$ mbar), over the range of 80−1880 ps with the corresponding simulation using the rotational and centrifugal distortion constants given in Table 4.

between the transitions with $\Delta J = \pm 2$ and ± 1, with different Clebsch-Gordan coefficients, whereas the half-integer recurrences involve $\Delta J = \pm 2$ transitions only.[36] Hence the integer recurrences have more complex shapes than the half-integer coherences.

With increasing delay time, each of the rotational coherences shows increasing spread. This is due to two contributions: (i) The effect of centrifugal distortion on the rotational energies (see eq 2), the high- J rotational states giving signal contributions at later delay than the low-J states. (ii) Contributions from the different thermally excited $v = 1$ states. The major part of each recurrence arise from the $v = 0$ ground state. The ν_{11}, ν_{17}, and ν_{22} and the degenerate ν_{41}/ν_{42} $v = 1$ levels have slightly larger rotational constants than $v = 0$, and contribute to each recurrence at earlier time, whereas the ν_6 $v = 1$ state has a smaller rotational constant and contributes at later time.

Figure 4a−f shows in detail the effect of the vibrational contributions of the ν_6, ν_{11}, ν_{17}, ν_{22}, and the degenerate ν_{41}/ν_{42} levels on the half-integer rotational recurrence 10.5: The $P^{(3)}(t)$ contributions of the $v = 0$ and 1 vibrationally excited states

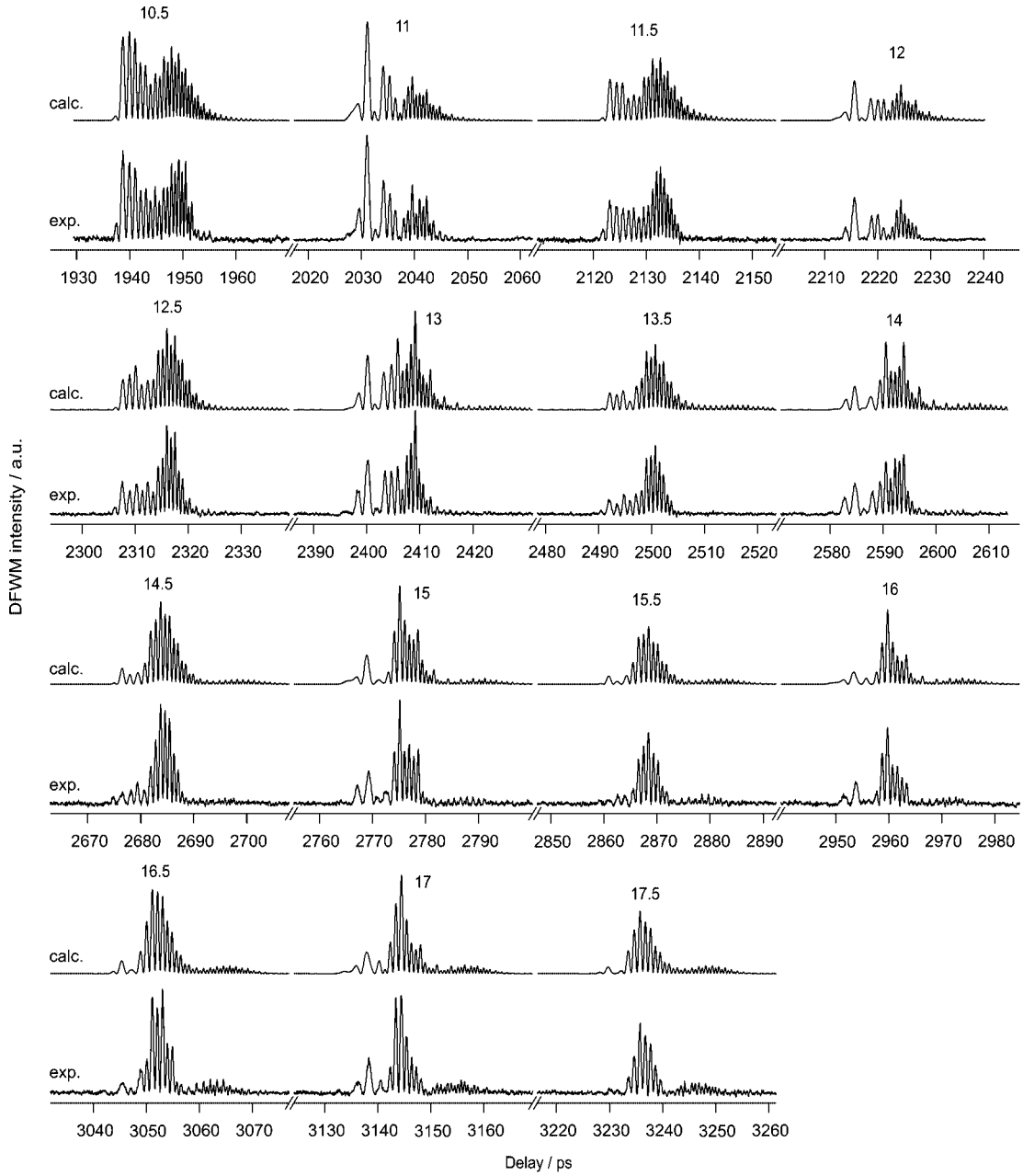

Figure 3. fs-DFWM rotational coherence transient of COT in a gas cell (295 K, $p = 3$ mbar), over the time range $t = 1930 - 3260$ ps with the corresponding simulation using the rotational and centrifugal distortion constants given in Table 4.

TABLE 4: Experimental and Calculated Rotational (MHz) and Centrifugal Distortion D_J and D_{JK} (Hz) Constants of Cyclooctatetraene for $v = 0$ and 1 Vibrational Levels

vibration	parameter[a]	fs-DFWM	$B_0 - B_v$	CW Raman[b]	CCSD(T)/ANO0[c]
v = 0	B_0	2 710.329(56)		2709.88(45)	2654.01
	D_J	561.7(55)		402(30)	524.5
	D_{JK}	−922(70)			−781.2
ν_6	B_1 (ν_6)	2708.54(14)	+1.79(14)		1.8702
ν_{11}	B_1 (ν_{11})	2710.65(19)	−0.32(19)		−0.0775
ν_{17}	B_1 (ν_{17})	2713.65(10)	−3.32(10)		−3.1196
ν_{22}	B_1 (ν_{22})	2712.19(24)	−1.86(24)		−1.1559
ν_{41}/ν_{42}	B_1 ($\nu_{41,42}$)	2711.21(23)	−0.88(23)		−0.9657
fitted J		0−140		0−43	

[a] D_J and D_{JK} constants for the excited vibrations are set to the $v = 0$ value. [b] Reference 28. [c] Excited state rotational constants given as $B_0 - B_v$.

add coherently to give the total $P^{(3)}(t)$ shown in Figure 4g. Taking the square norm $|P^{(3)}(t)|^2$ of (g) results in the simulated signal (h). Convolution of (h) with the 155 ps apparatus function results in the simulated recurrence (i), which can be compared to the experimental recurrence. In analogy to Figure 4, every recurrence of the transient can be fitted in great detail.

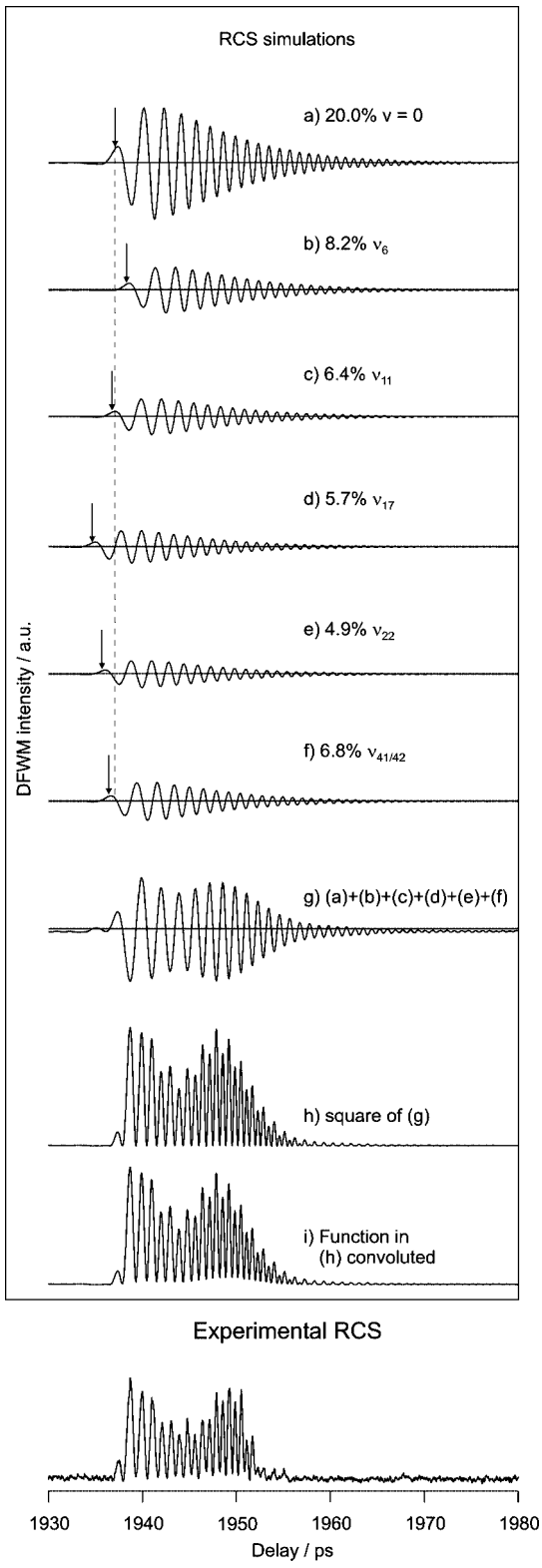

Figure 4. Effect of the $v = 0$ and thermally excited vibrational states of cyclooctatetraene on the recurrence no. 10.5, see also Figure 3. Traces a−f are calculated for the vibrational states $v = 0$, ν_6, ν_{11}, ν_{17}, ν_{22}, and $\nu_{41,42}$. The arrows indicate the 1/4B positions for the respective constants B_v. Trace g is the coherent addition of traces a−f. Trace h is the square of trace g, and trace i is the convoluted function of h.

Sections of the transient covering two half and full recurrences (i.e., 0.5−2, 2.5−4, etc.) were fitted individually. The B_0 value of the CW Raman experiment[28] and the D_J and D_{JK} and excited vibrational state values of the CCSD(T)/ANO0 calculation were taken as starting values for the fit. Rotational levels from $J =$ 0−140 were taken into account. The centrifugal distortion constants D_J and D_{JK} for the $v = 0$ state were limited to the ranges 0.50−0.56 and −0.90 to −0.50 kHz, respectively. The D_J and D_{JK} centrifugal distortion constants for the excited vibrational states were set to the $v = 0$ values. The fit was started with section 10.5−12, which exhibits rich temporal structure and a good signal/noise ratio. In the first cycle the fitting limits for the B_v constants were set to ±0.01% of the ab initio values. During the following cycles, the B_v limits were successively widened for each constant until all fitting parameters remained within the limits. The rotational constants and the limits thus obtained were then used as starting values and boundary conditions for the analysis of the other sections of the transient. For each fitting cycle, a subset of five fit variables was randomly selected, the others remaining fixed during that fitting cycle. The calculation of the mean values and (1 σ) standard deviations was performed with the six transient sections from recurrences 4.5−6 to 14.5−16, see Figures 2 and 3. The results are given in Table 4.

Table 4 lists the fitted rotational and centrifugal constants for COT. The $v = 0$ rotational constant B_0 is 2710.33(6) MHz. This is 0.45 MHz larger than the CW Raman value of Thomas and Weber (TW). [28] Note that TW fitted a single effective B constant that represents the thermal average of the rotational constants of the $v = 0$ and different $v = 1$ states; their B value cannot be directly compared to ours. In addition, TW were not able to spectrally resolve the K-sub-band structure and hence did not include the parameter D_{JK} in their fit. Also, their fit was only based on transitions up to $J \leq 43$, because of overlap between lines of the R and S branches.

The centrifugal distortion constant D_J is determined to be 561.7(55) Hz, which is 28% larger than that of TW,[28] probably due to the absence of D_{JK} in their fit. The sensitivity of the fit to D_{JK} is much smaller than to D_J, hence the 1 σ uncertainty of D_{JK} is 70 Hz or 8%. The CCSD(T) calculated D_J and D_{JK} values lie within ∼15% of the fitted values.

B. DFWM Measurements, Fitting, and Rotational Constants of C_8D_8. Although the COT-d_8 purification was not completely successful, the first three transients covering the recurrences 0.5−2, 2.5−4, and 4.5−6 exhibited signals from COT-d_8 only and could be fully analyzed. The later recurrences were partially influenced by the RCS transient of C_6D_6. Figure 5 shows an overview of the Raman RCS transient of C_8D_8 over the time ranges 100−1350 ps.

In addition to the same thermally populated vibrational states as for COT-h_8, the fit model for COT-d_8 took the $v = 2$ overtone of ν_6 into account. During the fitting procedure the $B(v)$ of the $v = 1$ and 2 excited states were constrained to the $B(v)/B_0$ ratios of the CCSD(T)/ANO0 calculation given in Table 5. This restriction was necessary, since the early recurrences do not show enough fine structure originating from the vibrationally excited states to allow significant fitting. The centrifugal distortion constants of the $v = 1$ and 2 vibrational states (D_v^J and D_v^{JK}) were set to the $v = 0$ values. As for COT-h_8, the range of fitted J states was 0−140.

The rotational and centrifugal distortion constants for the ground-state given in Table 5 are average values of the constants evaluated from the two transients covering the recurrences 2.5−4 and 4.5−6 listed in Table 5: the values in parentheses are the respective deviations. The data covering the recurrences 0.5−2 was not used for the fitting procedure because of the large deviation from the others. For COT the B_0 value resulting form the recurrences 2.5−4 is very close to the fitted B_0. Again the errors calculated by the fit program are much smaller than

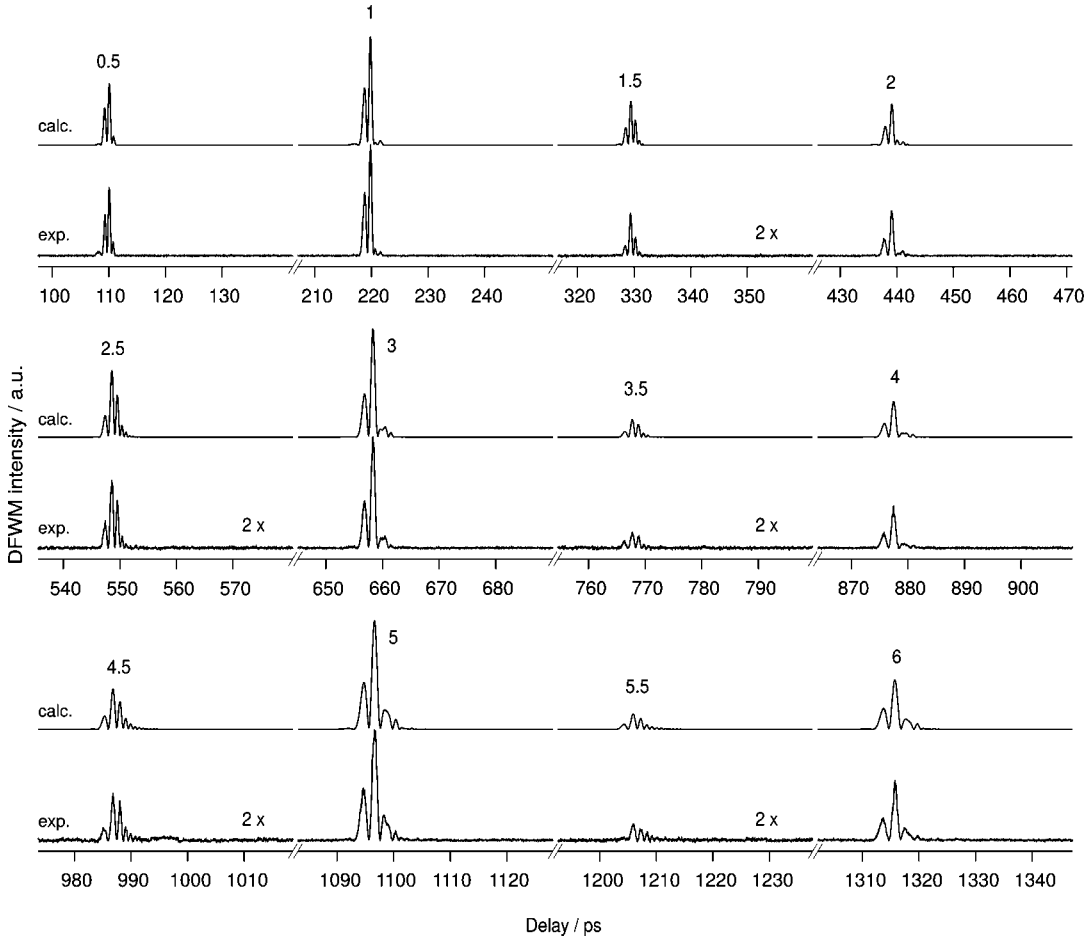

Figure 5. Femtosecond degenerate four-wave mixing (fs-DFWM) rotational coherence transient of cyclooctatetraene-d_8 in a gas cell (295 K, p = 3−5 mbar), over the range 100−1350 ps, using the rotational and centrifugal distortion constants given in Table 5.

TABLE 5: Experimental and Calculated Rotational (MHz) and Centrifugal Distortion D_J and D_{JK} (Hz) Constants of Cyclooctatetraene-d_8 for the $v = 0-2$ Vibrational Levels

vibration	parameter	fs-DFWM[a,b]	CCSD(T)/ANO0[c]
$v = 0$	B_0	2283.318(88)	2235.95
	D_J	369(28)	323.7
	D_{JK}	−639(78)	−472.4
ν_6, $v = 1$	B_1 (ν_6)		+1.1590
ν_{11}, $v = 1$	B_1 (ν_{11})		−0.0581
ν_{17}, $v = 1$	B_1 (ν_{17})		−1.7403
ν_{22}, $v = 1$	B_1 (ν_{22})		−1.0083
ν_{41}/ν_{42}, $v = 1$	B_1 ($\nu_{41,42}$)		+0.8750
ν_6, $v = 2$	B_2 (ν_6)		+2.318
fitted J		0−140	

[a] B_v values are taken from the CCSD(T)/ANO0 calculation for v = 1 states. [b] D_J and D_{JK} of the excited vibrations are constrained to the $v = 0$ values. [c] Excited state rotational constants given as $B_0 - B_v$.

the overall 1 σ errors obtained by the statistical evaluation of the two transients.

The ground-state rotational constant B_0 is 2 283.318(88) MHz. Although there is a very good agreement between experiment and calculation, see Figure 5, the B_0 value could not be determined to higher precision due to the lack of unperturbed recurrences for delay times t > 1340 ps. D_J could be determined to 369(28) Hz and D_{JK} to −639(78) Hz. The D_J value is about ten times less precise than the value obtained for COT-h_8, whereas the D_{JK} value has almost the same precision. The centrifugal distortion constants lie within ∼26% of the CCSD(T) calculated values. The experimental as well as the calculated results are summarized in Table 5.

C. Vibrationally Excited States. The ν_6 (a_1) vibration is the "tub distortion" mode (see Figure 6). For large displacement amplitudes it leads to the planar form of COT and further to the symmetry-equivalent "down" tub form. It is the only vibrational state of COT investigated here that has a smaller rotational constant than the ground state. The ν_{11} (a_2) vibration is a ring-twisting mode and induces only a very small relative change of rotational constant (5×10^{-5}). The ν_{17} (b_1) vibration is a C═C−C═C ring deformation combined with H−C−C−H torsion around the single bonds. Of the six states investigated, this vibration results in the largest increase of the rotational constant, 3.3 MHz or 0.11% relative to B_0. The ν_{22} (b_2) vibration is also a C═C−C═C ring deformation, but involves conrotation of the H−C═C−H subunits. The degenerate vibration (ν_{41} and ν_{42}, e) involves ring twisting plus H−C−C−H torsion around the single bonds, and leads to a small increase of the rotational constant. Descriptions of the COT normal modes have also been given by Perec.[27]

V. Discussion

We have previously described a combined experimental/theoretical extrapolation method for determining the molecular equilibrium structure s_e.[52,53] Figure 7 shows the result of such an extrapolation for the C−C equilibrium bond length for both COT and COT-d_8. Based on the CCSD(T)/cc-pVXZ (X = 2, 3) calculations, we plot the equilibrium rotational constant B_e vs the calculated C−C equilibrium bond distances, the dashed

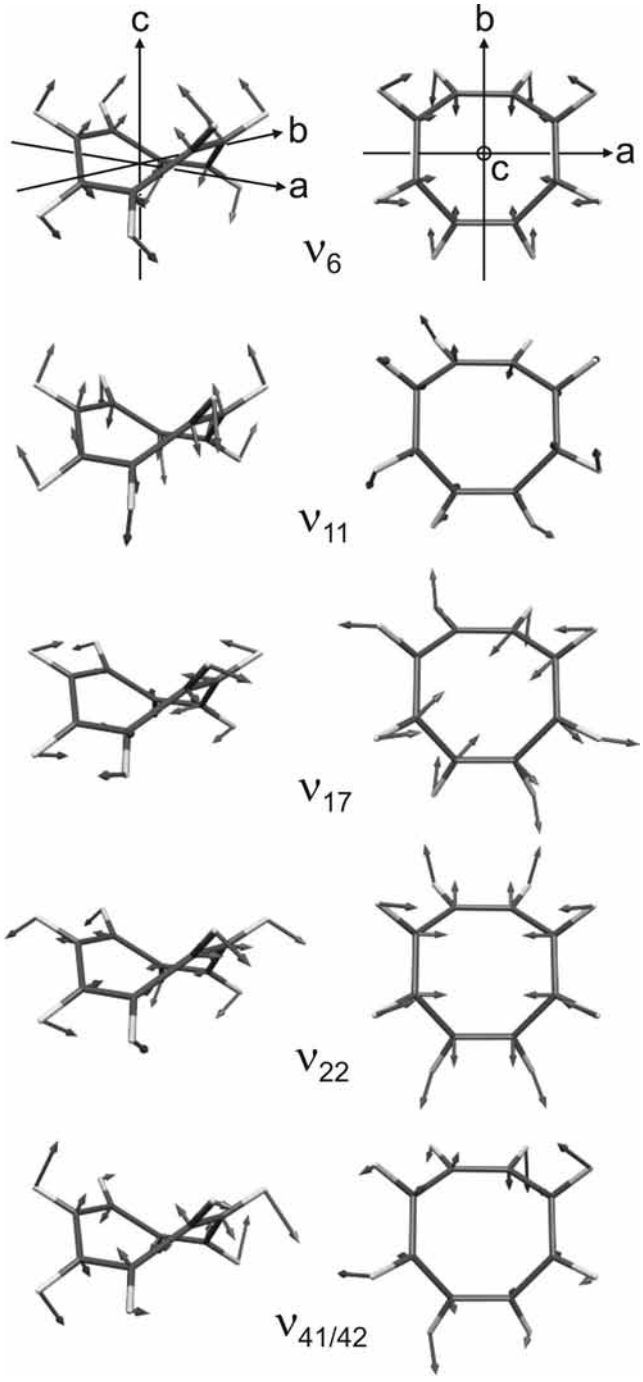

Figure 6. Normal mode eigenvectors for the thermally excited vibrations ν_6, ν_{11}, ν_{17}, ν_{22}, and ν_{41}, side and top view. The top row also shows the molecule-fixed rotational axes and the respective rotational constants.

line connecting the cc-pVDZ and cc-pVTZ values. To obtain the analogous correlation of equilibrium distance with the vibrationally averaged rotational constant $B_{0,\mathrm{calc}}$, we calculated the difference of B_e and B_0, $\Delta(B_e - B_0)$, by second-order perturbation theory at the CCSD(T)/ANO0 level (see section II.B). The respective B_e and B_0 values in Figure 7 are connected by vertical dotted lines.

The desired quantity for comparison with the experimental B_0 is the complete basis set (CBS) vibrationally averaged rotational constant $B_{0,\mathrm{CBS}}$, which for a perfect ab initio method and infinite basis set should coincide with the experimental value B_0. Since it is not yet computationally possible to perform a

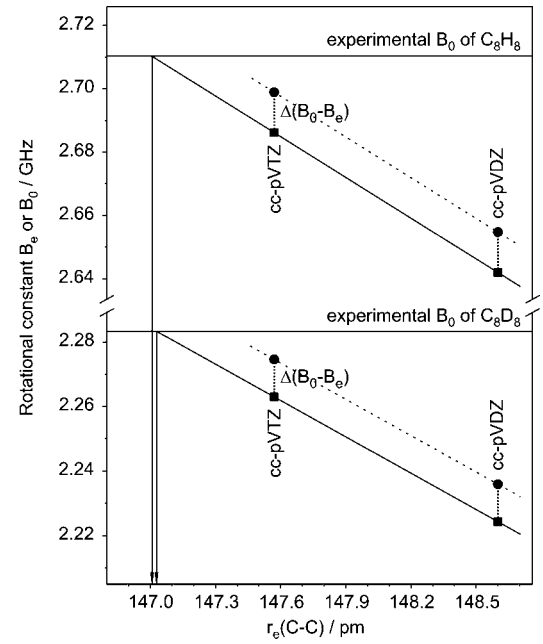

Figure 7. CCSD(T) calculated rotational constants B_e and B_0 plotted vs the C−C equilibrium bond length, using the cc-pVDZ and cc-pVTZ basis sets. Dashed lines connect the B_e values (●), solid lines connect the B_0 values (■). The $\Delta(B_e - B_0)$ values (dotted vertical lines) were calculated at the CCSD(T)/ANO0 level. The fs-DFWM experimental B_0 is drawn as horizontal line. The intersections of the calculated and experimental solid lines give the C−C equilibrium bond length.

CBS extrapolation of the $B_{0,\mathrm{calc}}$ values to very large basis sets, we instead extrapolate the cc-pVDZ and cc-pVTZ values to the experimental $B_{0,\mathrm{exp}}$ by the solid lines in Figure 7. These extrapolations yield the CCSD(T) estimates of the C−C equilibrium bond lengths. The values for the C═C and C−H equilibrium bond lengths and for the equilibrium angles α_e (C−C−C), β_e (H−C═C), and γ_e (H−C−C), were obtained by analogous extrapolations and are given in Table 6.

The errors associated with the values extrapolated in this way reflect on one hand the error in the determination of $B_{0,\mathrm{exp}}$, on the other hand the remaining imperfections of the CCSD(T) treatment, specifically (a) the lack of higher-order coupled-cluster terms (full triples, quadruples, etc.), (b) the noninclusion of core-valence correlation contributions, and (c) the lack of inclusion of relativistic effects. Within the Born−Oppenheimer approximation, the equilibrium structure is the same for all isotopic species. Any differences between the equilibrium values extrapolated for COT and COT-d_8 (as in Figure 7) are due to (i) errors in the determination of $B_{0,\mathrm{exp}}$, (ii) the incompleteness of the second-order perturbation theoretical calculation of $\Delta(B_e - B_0)$, and (iii) errors arising from the extrapolation from the $\Delta(B_e - B_0)$ values calculated with the finite cc-pVDZ and cc-pVTZ basis sets to complete basis set. We believe that the error contribution from (i) is much smaller than those from (ii) and (iii).

The equilibrium parameters given in Table 6 are the average of the equilibrium bond lengths and angles values determined for COT and COT-d_8. The error is estimated as five times the difference of the COT and COT-d_8 values from this average. The equilibrium bond lengths so derived are 133.7 ± 0.1 pm for the C═C double bond, 147.0 ± 0.05 pm for the C−C single bond, and 107.9 ± 0.1 pm for the C−H bond.

An interesting comparison to 1,3,5,7-COT is afforded by 1,3-butadiene, since both molecules have C═C double bonds and C−C bonds between the sp^2-hybridized carbon atoms. Two

TABLE 6: Equilibrium Structure Parameters of Cyclooctatetraene and Cyclooctatetraene-d_8

method	fs-DFWM/ab initio	CCSD(T)cc-pVTZ	CCSD(T)cc-pVDZ	CCSD(T)ANO0	MP2cc-pVTZ	MP2cc-pVDZ
r_e (C−C) [pm]	147.02 ± 0.05	147.57	148.60	148.28	146.54	147.66
r_e (C=C) [pm]	133.71 ± 0.1	134.45	135.83	135.35	134.36	135.71
r_e (C−H) [pm]	107.94 ± 0.1	108.70	110.11	109.39	108.53	109.94
α_e (C−C−C) [deg.]	126.55 ± 0.01	126.47	126.33	126.55	126.06	125.97
β_e (H−C=C) [deg.]	117.698 ± 0.004	117.73	117.79	117.74	117.63	117.69
γ_e (H−C−C)[deg.]	115.613 ± 0.005	115.65	115.72	115.57	116.11	116.14

studies have explicitly addressed this comparison: A 1967 electron diffraction study of Haugen and Traetteberg found the C=C distance to be 0.4 pm shorter in COT than in butadiene (134.0 vs 134.4 pm) and the C−C distance to be 0.9 pm longer in COT (147.6 vs 146.7 pm).[22] However, they noted that the differences were of the same order of magnitude as their experimental error limits, 0.3−0.4 pm and did not claim significance for these differences.[22] Recently, improved equilibrium geometry bond lengths of *s-trans*-butadiene have been determined by Craig et al., by adjusting the constants obtained from rotational spectroscopy using vibration−rotation constants calculated at the MP2 and B3LYP quantum chemical levels.[72] This investigation yielded r_e (C−C) = 145.4(1) pm, r_e (C=C) = 133.8(1) pm, and r_e (C−H) = 107.9(1) pm.[72]

Upon comparison with the values given in Table 6, one sees that the equilibrium C=C bond lengths of *s-trans*-butadiene and cyclooctatetraene are equal within the ±0.1 pm error limit. This is very interesting, since it implies that the lengthening of the C=C double bond relative to ethene, for which r_e (C=C) is 133.07 pm,[72−74] is 0.6 pm for both for butadiene and COT. In many organic chemistry textbooks, the slight lengthening of the formal double bond in going from ethene to butadiene is used to introduce the concept of π-electron delocalization. Direct application of this qualitative idea would imply that the π electrons in COT are delocalized to the same extent as in *trans*-1,3-butadiene. However, since the angle between the *p* orbitals of adjacent single-bonded carbon atoms in COT is about 43°, the π electrons in COT should delocalize less well than in planar 1,3-butadiene, which is somewhat contradictory.

The equilibrium C−C bond length of COT (Table 6) is 1.6 pm longer than that of *trans*-1,3-butadiene.[72] This implies a slightly lower bond order of the formal C−C single bond in COT compared to butadiene, and is in line with the expected effect of the 43° twist angle on the π-electron delocalization. We note that the C−C bond length in COT (Table 6) is equal to the estimated length of a "localized" sp^2-sp^2 bond (147.0 pm),[72,75,76] implying that the C−C single bond in COT is fully localized. We conclude that the expected effect of decreased π-electron delocalization due to the twisting of adjacent C=C double bonds in COT relative to butadiene is observed for the C−C bonds but not for the C=C bonds.

VI. Conclusions

The rotational and centrifugal constants of COT and COT-d_8 have been accurately measured using the femtosecond rotational Raman coherence technique, detected by degenerate four-wave mixing. For COT, rotational coherence transients have been recorded over a total delay time of ~3.3 ns. These yield the rotational and centrifugal constants for the vibrational ground state, as well as the B_v rotational constants for ν_6, ν_{11}, ν_{17}, ν_{22}, and ν_{41}/ν_{42} $v = 1$ excited vibrational states. For COT the analysis yields the rotational constants of the six vibrational states with a relative accuracy of $\sim 5 \times 10^{-6}$. This about 10 times more accurate than obtained by high-resolution Raman spectroscopy.[28] For COT-d_8 the analysis yields the ground-state rotational constant with a relative accuracy of $\sim 8 \times 10^{-6}$.

We have also performed ab initio CCSD(T) calculations of the equilibrium as well as the vibrationally averaged rotational constants, using the ANO0 and cc-pVXZ ($X = 2, 3$) basis sets. Combination of the CCSD(T) results with the experimental B_0 allows us to determine the six independent equilibrium structural parameters [the C−C, C=C, and C−H bond lengths and the angles α_e (C−C−C), β_e (H−C=C), and γ_e (H−C−C)] of the gas-phase cyclooctatetraene molecule to very high accuracy.

The comparison of the equilibrium C−C and C=C bond lengths of COT with those of *trans*-1,3 butadiene reveals that the C−C single bond is 1.6 pm longer, whereas the C=C double bond length is identical within experimental error (±0.1 pm).[72] The decrease of π -electron delocalization on going from butadiene to COT should lead to an increase of the C−C bond length, it also predicts a contraction of the C=C bond length of COT, which is not observed. We emphasize that the effect of partial π-electron delocalization on the length of formal C=C bonds is very small (as exemplified by the 0.6 pm contraction between ethene and 1,3-butadiene[72]) and may be compensated by other stereoelectronic effects in the case of COT.

Acknowledgment. Financial support from the Schweiz. Nationalfonds through Grant No. 200020−112271 is gratefully acknowledged. J.F.S. acknowledges funding through the U.S. National Science Foundation and the U.S. Department of Energy, Basis Energy Sciences Division. Dr. Juana Vazquez is also thanked for running some calculations.

References and Notes

(1) Domenicano, A.; Hargittai, I. *Accurate Molecular Structures*; Oxford University Press: New York, 1992.
(2) Pratt, D. W. *Annu. Rev. Phys. Chem.* **1998**, *49*, 481.
(3) Durig, J. R. *Equilibrium Structural Parameters*; Elsevier: Amsterdam, 2000; Vol. 24.
(4) Coulson, C. A.; Moffitt, W. E. *Philos. Mag.* **1949**, *40*, 1.
(5) Lippincott, E. R.; Lord, R. C. *J. Am. Chem. Soc.* **1946**, *68*, 1868.
(6) Lippincott, E. R.; Lord, R. C.; McDonald, R. S. *J. Chem. Phys.* **1948**, *16*, 548.
(7) Lippincott, E. R.; Lord, R. C.; McDonald, R. S. *Nature* **1950**, *166*, 227.
(8) Lippincott, E. R.; Lord, R. C.; McDonald, R. S. *J. Am. Chem. Soc.* **1951**, *73*, 3370.
(9) Ahlers, G.; Hornig, J. F. *J. Am. Chem. Soc.* **1961**, *65*, 2102.
(10) Hrovat, D. A.; Borden, W. T. *J. Am. Chem. Soc.* **1992**, *114*, 5879.
(11) Andres, J. L.; Castano, O.; Morreale, A.; Palmeiro, R.; Gomperts, R. *J. Chem. Phys.* **1998**, *108*, 203.
(12) Castano, O.; Notario, R.; Gomperts, R.; Abboud, J. L. M.; Palmeiro, R.; Andres, J. L. *J. Phys. Chem. A* **1998**, *102*, 4949.
(13) Klärner, F.-G. *Angew. Chem., Int. Ed.* **2001**, *40*, 3977.
(14) Castano, O.; Palimero, R.; Frutos, L. M.; Luisandrés, J. *J. Comput. Chem.* **2002**, *23*, 732.
(15) Blancafort, L.; Bearpark, M. J.; Robb, M. A. *Mol. Phys.* **2006**, *104*, 2007.
(16) Wenthold, P. G.; Hrovat, D. A.; Borden, W. T.; Lineberger, W. C. *Science* **1996**, *272*, 1456.
(17) Bastiansen, O.; Hassel, O.; Langseth, A. *Nature* **1947**, *160*, 128.
(18) Bastiansen, O.; Hassel, O. *Acta Chem. Scand.* **1949**, *3*, 209.
(19) Karle, I. L. *J. Chem. Phys.* **1952**, *20*, 65.
(20) Bastiansen, O.; Hedberg, L.; Hedberg, K. *J. Chem. Phys.* **1957**, *27*, 1311.
(21) Trætteberg, M. *Acta Chem. Scand.* **1966**, *20*, 1724.

(22) Haugen, W.; Trætteberg, M. *Selected Topics in Structure Chemistry*; Andersen, P., Bastiansen, O., Furberg, S., Eds.; Universitetsforlaget: Oslo, 1967.
(23) Kaufman, H. S.; Fankuchen, I.; Mark, H. *Nature* **1948**, *161*, 165.
(24) Claus, K. H.; Krüger, C. *Acta Crystallogr., Sect. C* **1988**, *44*, 1632.
(25) Flett, M. S.; Cave, W. T.; Vago, E. E.; Thompson, H. W. *Nature* **1947**, *159*, 739.
(26) Saskena, B. D.; Narain, H. *Nature* **1950**, *165*, 723–723.
(27) Perec, M. *Spectrochim. Acta, Part A* **1991**, *47*, 799.
(28) Thomas, P. M.; Weber, A. *J. Raman Spectrosc.* **1978**, *7*, 353.
(29) Zhou, X.; Liu, R.; Pulay, P. *Spectrochim. Acta, Part A* **1993**, *49*, 953.
(30) Santos, H. F. D.; Rocha, W. R.; De Almeida, W. B. *Chem. Phys.* **2002**, *280*, 31.
(31) Bearpark, M. J.; Blancafort, L.; Robb, M. A. *Mol. Phys.* **2002**, *100*, 1735.
(32) Frutos, L. M.; Castano, O.; Merchan, M. *J. Phys. Chem. A* **2003**, *107*, 5472.
(33) Petryk, M. W. P.; Henry, B. R. *J. Phys. Chem. A* **2005**, *109*, 7113.
(34) Felker, P. M.; Zewail, A. H. *J. Chem. Phys.* **1987**, *86*, 2460.
(35) Felker, P. M. *J. Phys. Chem.* **1992**, *96*, 7844.
(36) Felker, P. M.; Zewail, A. H. Molecular Structures from Ultrafast Coherence Spectroscopy. In *Femtosecond Chemistry*; Manz, J., Wöste, L., Eds.; VCH: Weinheim, Germany, 1995; Vol. I, Chapter 5.
(37) Frey, H. M.; Beaud, P.; Gerber, T.; Mischler, B.; Radi, P. P.; Tzannis, A. P. *Appl. Phys. B: Laser Opt.* **1999**, *68*, 735.
(38) Brown, E. J.; Zhang, Q.; Dantus, M. *J. Chem. Phys.* **1999**, *110*, 5772.
(39) Lang, T.; Frey, H. M.; Beaud, P.; Motzkus, M. In *Raman Spectroscopy*; Zhang, S.-L., Zhu, B.-F., Eds.; John Wiley: New York, 2000.
(40) Lang, T.; Beaud, P.; Frey, H. M.; Motzkus, M. *J. Chem. Phys.* **2001**, *115*, 5418.
(41) Frey, H. M.; Beaud, P.; Gerber, T.; Mischler, B.; Radi, P. P.; Tzannis, A. P. *J. Raman Spectrosc.* **2000**, *31*, 71.
(42) Frey, H. M.; Beaud, P.; Lang, T.; Motzkus, M. *Femtochemistry and Femtobiology, Ultrafast Dynamics in Molecular Science*; Douhal, A., Santamaria, J., Eds.; World Scientific Publishing: Singapore, 2002; Chapter 1.
(43) Frey, H. M.; Müller, A.; Leutwyler, S. *J. Raman Spectrosc.* **2002**, *33*, 855.
(44) Jarzeba, W.; Matylitsky, V. V.; Weichert, A.; Riehn, C. *Phys. Chem. Chem. Phys.* **2002**, *4*, 451.
(45) Matylitsky, V. V.; Jarzerba, W.; Riehn, C.; Brutschy, B. *J. Raman Spectrosc.* **2002**, *33*, 877.
(46) Jarzeba, W.; Matylitsky, V.; Riehn, C.; Brutschy, B. *Chem. Phys. Lett.* **2003**, *368*, 680.
(47) Riehn, C.; Matylitsky, V.; Jarzeba, W.; Brutschy, B.; Tarakeshwar, P.; Kim, K. *J. Am. Chem. Soc.* **2003**, *125*, 16455.
(48) Riehn, C.; Matylitsky, V. V.; Gelin, M. F. *J. Raman Spectrosc.* **2003**, *34*, 1045.
(49) Frey, H. M.;. Kummli, D.;. Keller, M.;. Leist, R.;. Leutwyler, S. Femtosecond degenerate four-wave mixing of cycloalkanes. In *Femtochemistry and Femtobiology*; Martin, M. M., Hynes, J. T., Eds.; Elsevier: Amsterdam, 2004.
(50) Kummli, D. S.; Frey, H. M.; Keller, M.; Leutwyler, S. *J. Chem. Phys.* **2005**, *123*, 054308.
(51) Kummli, D. S.; Frey, H. M.; Leutwyler, S. *Chimia* **2006**, *60*, 212.
(52) Kummli, D. S.; Frey, H. M.; Leutwyler, S. *J. Chem. Phys.* **2006**, *124*, 144307.
(53) Kummli, D. S.; Frey, H. M.; Leutwyler, S. *J. Phys. Chem. A* **2007**, *111*, 11936.
(54) Purvis III, G. D.; Bartlett, R. J. *J. Chem. Phys.* **1982**, *76*, 1910.
(55) Raghavachari, K.; Trucks, G. W.; Pople, J. A.; Head-Gordon, M. *Chem. Phys. Lett.* **1989**, *157*, 479.
(56) Scuseria, G. E. *J. Chem. Phys.* **1991**, *42*, 442.
(57) Almlöf, J.; Taylor, P. R. *J. Chem. Phys.* **1987**, *86*, 4070.
(58) Vázquez, J.; Stanton, J. F. *Mol. Phys.* **2006**, *104*, 377.
(59) Stanton, J. F.; Lopreore, C. L.; Gauss, J. *J. Chem. Phys.* **1998**, *108*, 7190.
(60) Stanton, J. F.; Gauss, J.; Watts, J. D.; Szalay, P. G.; Bartlett, R. J., with contribution fromAuer A. A. ; Bernholdt, D. B.; Christiansen O.; Harding, M. E. ; Heckert, M.; Heun, O.; Huber, C. ; Jonsson, D. ; Juselius, J.; Lauderdale W. J.; Metzroth, T.; Michauk, C.; O'Neill D. P.; Price, D. R.; Ruud, K.; Schiffmann, F. ; Varner, M. E. ; Vazquez, J. *the integral packages MOLECULE* (Almloef J. and Taylor P. R.), PROPS (P. R. Taylor), and ABACUS (Helgaker, T. Aa.Jensen, H. J. Jorgensen, P. and Olsen J.). For the current version, see www.aces2.de
(61) Shen, Y. R. *The Principles of Nonlinear Optics*; John Wiley & Sons: New York, 1984.
(62) Mukamel, S. *Principles of Nonlinear Spectroscopy*; Oxford University Press: New York, 1995.
(63) Boyd, R. W. *Nonlinear Optics*; Academic Press: New York, 2003.
(64) Grimberg, B.; Lozovoy, V.; Dantus, M.; Mukamel, S. *J. Phys. Chem. A* **2002**, *106*, 697.
(65) The GAP group, GAP - Groups, Algorithms and Programming, Version 4.4.6, 2005 (http://www-gap.dcs.st-and.ac.uk/).
(66) Schmied, R.; Lehmann, K. K. *J. Mol. Spectrosc.* **2004**, *226*, 201.
(67) Weber, A. *J. Chem. Phys.* **1980**, *73*, 3952.
(68) Hegelund, F.; Rasmussen, F.; Brodersen, S. *J. Raman Spectrosc.* **1973**, *1*, 433.
(69) Brodersen, S. In *High resolution rotational-vibrational Raman Spectroscopy*; Weber, A., Ed.; Springer Verlag: Berlin, 1978; Chapter 2.
(70) Polanyi, J. C.; Woodall, K. B. *J. Chem. Phys.* **1971**, *56*, 1563.
(71) Procaccia, I.; Levine, R. *J. Chem. Phys.* **1975**, *63*, 4261.
(72) Craig, N. C.; Groner, P.; McKean, D. C. *J. Phys. Chem. A* **2006**, *110*, 7461.
(73) Bak, K. L.; Gauss, J.; Jorgensen, P.; Olsen, J.; Helgaker, T.; Stanton, J. F. *J. Chem. Phys.* **2001**, *114*, 6548.
(74) Pawlowski, F.; Jorgensen, P.; Olsen, J.; Hegelund, F.; Helgaker, T.; Gauss, J.; Bak, K. L.; Stanton, J. F. *J. Chem. Phys.* **2002**, *116*, 6482.
(75) Dewar, M. J. S.; Schmeising, H. N. *Tetrahedron* **1959**, *5*, 166.
(76) Harmony, M. D. In *Vibrational Spectra and Structure*; Durig, J. M., Ed.; Elsevier: Amsterdam, 2000.

JP803523Y